Experimental Landau-Zener Tunneling for Wave Redirection in Nonlinear Waveguides

Chongan Wang,[1] Ali Kanj,[1] Alireza Mojahed,[1] Sameh Tawfick,[1,2,*] and Alexander F. Vakakis[1]

[1] *Department of Mechanical Science and Engineering, University of Illinois at Urbana-Champaign, Champaign, Illinois 61801, USA*

[2] *The Beckman Institute for Advanced Science and Technology, University of Illinois at Urbana-Champaign, Champaign, Illinois 61801, USA*

(Received 22 June 2020; revised 29 July 2020; accepted 19 August 2020; published 21 September 2020)

We present an acoustic analog of the Landau–Zener-tunneling (LZT) quantum-mechanical effect and apply it for irreversible wave redirection in weakly coupled nonlinear waveguides under impulse excitation. Due to nonlinearity, LZT-induced wave redirection is passively self-tunable with energy, being realized only in a certain energy band, which can be precisely predicted by theoretical models. Apart from the macroscale experimental validation of the classical quantum LZT effect, the findings apply to a broad class of acoustical systems with nonlinearity, disorder, and weak coupling.

DOI: 10.1103/PhysRevApplied.14.034053

I. INTRODUCTION

Landau-Zener tunneling (LZT) denotes nonadiabatic energy tunneling in a quantum-mechanical system, across an energy gap between two anticrossed energy levels [1,2]. LZT has been observed in various fields, including semiconductor superlattices [3,4], optical fields [5,6], Bose-Einstein condensates [7,8], ultrasonic superlattices [9], phononic crystals [10,11], and surface elastic waves [12]. The common feature in these applications is the intriguing irreversible resonance-induced energy transition between two states under external stimulation or perturbation. Perhaps the simplest analog of quantum LZT in classical mechanics is in two weakly coupled identical pendulums; when one of the pendulum lengths slowly varies, irreversible energy transfer occurs between the pendulums due to parametric resonance [13,14].

Here, we provide experimental validation of a macroscale LZT analog in space for a system of two weakly coupled and disordered nonlinear waveguides under impulsive excitation. Recently, it has been theoretically shown [15,16] that LZT can yield to wave redirection in this system. Specifically, a symmetry-breaking variation of the spatial stiffness distribution in one of the waveguides induces LZT in space, resulting in irreversible breather redirection from the directly excited waveguide to the other. A break of symmetry is necessary for LZT, as in its absence wave localization [17–19] or recurrent wave exchanges [17–20] are realized. Analysis reduces the nonlinear acoustics of the coupled waveguides to a model of coupled oscillators with time-varying stiffness, enabling crossing eigenfrequencies in the time and resonance capture [16]. Moreover, due to nonlinearity, the LZT-based wave redirection proves to be self-tunable to the intensity of the impulse and is realized only within a certain energy band; otherwise, wave localization occurs [16].

Apart from the experimental demonstration of a macroscale analog in space of LZT, we confirm the efficacy of passive wave redirection in a system of impulsively excited acoustic waveguides with nonlinearity, weak coupling, and spatial disorder. In addition, we highlight the self-tunability of LZT-based wave redirection to input energy, rendering the acoustical system passively self-adaptive to the external stimulant. Our experiments corroborate previous theoretical predictions and enable tunable-with-energy acoustic systems with an inherent capacity for wave redirection.

II. LZT IN THE REDUCED-ORDER MODEL (ROM)

The ROM of Fig. 1(a) consists of two waveguides, each with $n = 7$ unit cells. We refer to the waveguide the first unit cell of which is subjected to an ideal impulse as an excited waveguide with unit cells E1–E7 and to the other as an absorbing waveguide with unit cells A1–A7. Each unit cell is composed of a linearly grounded oscillator, coupled by essentially (i.e., nonlinearizable) nonlinear springs to its adjacent unit cells in the same waveguide, and by weak linear springs to the corresponding unit cell in the other waveguide. The equations of motion are as follows:

$$m\ddot{x}_1 + c_{g1}\dot{x}_1 + k_{g1}x_1 + k_e(x_1 - y_1) + c_e(\dot{x}_1 - \dot{y}_1) + c_{nl}(\dot{x}_1 - \dot{x}_2) + k_{nl}|x_1 - x_2|^{\beta-1}(x_1 - x_2) = F(t), \tag{1a}$$

*tawfick@illinois.edu

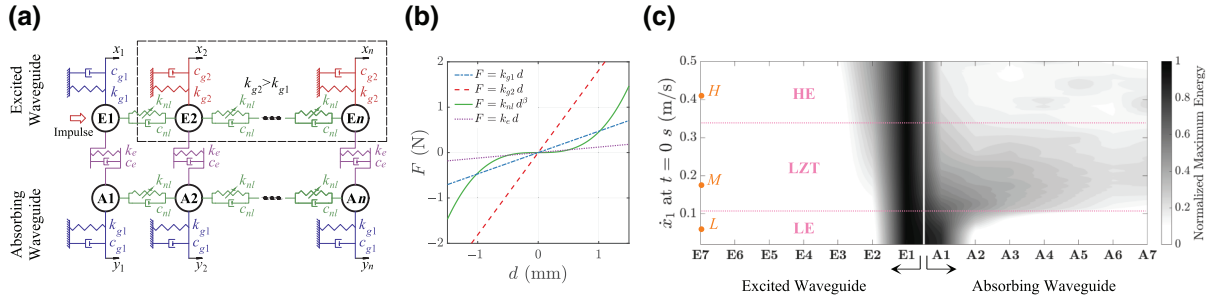

FIG. 1. The theoretical study of macroscale Landau-Zener tunneling (LZT) in space. (a) A schematic of the reduced-order-model (ROM). (b) The force-displacement relations for the stiffnesses used. (c) The energy penetration in the 14-unit-cell ROM (see Table I for parameters) for varying initial velocity imposed on unit cell E1; this is represented by contour levels of maximum normalized energy (with respect to the input energy) of each unit cell, with three distinct penetration regimes detected, namely, low energy (LE point L), intermediate energy (IE point M), and high energy (HE point H).

$$m\ddot{x}_i + c_{g2}\dot{x}_i + k_{g2}x_i + k_e(x_i - y_i) + c_e(\dot{x}_i - \dot{y}_i) + c_{nl}(\dot{x}_i - \dot{x}_{i-1}) + c_{nl}(\dot{x}_i - \dot{x}_{i+1}) + k_{nl}|x_i - x_{i-1}|^{\beta-1}(x_i - x_{i-1}) + k_{nl}|x_i - x_{i+1}|^{\beta-1} \times (x_i - x_{i+1}) = 0, \quad 2 \leqslant i \leqslant n = 7, \tag{1b}$$

$$m\ddot{y}_i + c_{g1}\dot{y}_i + k_{g1}y_i + k_e(y_i - x_i) + c_e(\dot{y}_i - \dot{x}_i) + c_{nl}(\dot{y}_i - \dot{y}_{i-1}) + c_{nl}(\dot{y}_i - \dot{y}_{i+1}) + k_{nl}|y_i - y_{i-1}|^{\beta-1}(y_i - y_{i-1}) + k_{nl}|y_i - y_{i+1}|^{\beta-1} \times (y_i - y_{i+1}) = 0, \quad 1 \leqslant i \leqslant n = 7, \tag{1c}$$

with $y_0 \overset{\text{def}}{=} y_1$, $x_8 \overset{\text{def}}{=} x_7$, and $y_8 \overset{\text{def}}{=} y_7$, which denote the free boundary conditions of the boundary cells A1, E7, and A7; the boundary cell E1 is the one that is excited by the impulse $F(t) = I\delta(t)$, where $\delta(t)$ is the Dirac delta function and I is the intensity of the impulse. Moreover, assuming zero initial conditions, the applied impulse is equivalent to the initial condition $\dot{x}_1(0+) = I/m$ for unit cell E1. In Eq. (1), m denotes the mass and k_{g1} and k_{g2} the stiffnesses of the softer and stiffer linear groundings, respectively. The first unit cell of the excited waveguide and all unit cells of the absorbing one possess softer grounding stiffnesses, $k_{g1} < k_{g2}$, breaking the symmetry. Also, c_{g1} and c_{g2} are the viscous damping coefficients of the soft and stiff groundings, respectively, whereas damping in the linear couplers is neglected: $c_e \sim 0$ (see the Supplemental Material [21]). Lastly, k_{nl}, β, and c_{nl} are the stiffness coefficient, exponent, and linear damping coefficient of the nonlinear intrawaveguide coupling, respectively, and k_e is the stiffness of the linear interwaveguide coupling. These are estimated by experimental system identification [21–26] and are given in Table I. The listed values and respective bracketed values (where applicable) are the mean and standard deviations of the identified parameters, respectively; otherwise, the listed values are typical identified parameters.

For no spatial disorder, there are recurrent propagating breather exchanges [27] in the two waveguides, in a nonlinear beat phenomenon. With spatial disorder added, this evolves to irreversible breather redirection from the excited to the absorbing waveguide due to LZT [16]. This is shown by assuming a regime of irreversible breather redirection and introducing the variables

$$u = \sum_{i=1}^{7} x_i; \quad v = \sum_{i=1}^{7} y_i. \tag{2}$$

Omitting damping, summing Eqs. (1), and applying Eq. (2), the following linear system is obtained:

$$m\ddot{u} + k_{gE}(t)u + k_e(u - v) = 0, \tag{3a}$$

$$m\ddot{v} + k_{g1}v + k_e(v - u) = 0, \tag{3b}$$

where u and v denote the excited and absorbing effective oscillators, respectively. The symmetry-breaking time-varying stiffness $k_{gE}(t)$ in Eq. (3a) reflects the change in the effective grounding stiffness as the breather propagates within the excited waveguide [15,16] and converts

TABLE I. The parameters of the ROM given in Eq. (1).

m (kg)	k_{g1} (N/m)	k_{g2} (N/m)	k_e (N/m)	c_{g1} (Ns/m)	c_{g2} (Ns/m)	k_{nl} (N/m$^\beta$)	β	c_{nl} (Ns/m)
0.0245	470.25 [30.35]	1813.2 [39.3]	121.17 [8.30]	0.0219 [0.007]	0.0359 [0.0154]	2.3×10^8	2.902	0.0161

the spatial disorder in Eq. (1) into temporal disorder in Eq. (3). Note that, initially, the grounding stiffness of the excited effective oscillator is equal to the uniform grounding stiffnesses of the unit cells of the absorbing waveguide, $k_{gE}(t) \to k_{g1}$, whereas it subsequently increases to the value $k_{gE}(t) \to k_{g2}$ with increasing time. Therefore, the coupled effective oscillators (3a) and (3b) have two distinct time-dependent eigenstates; these eigenstates enable an initial 1:1 resonance capture between the two effective oscillators and a subsequent escape from resonance capture as time progresses. The time scales governing the resonance capture and escape are governed by the weak coupling $k_e \ll \min\{k_{g1}, k_{g2}\}$ and the strong spatial stiffness disorder $k_e \ll |k_{g2} - k_{g1}|$. Based on these observations, a three-stage model is created in Ref. [16] to analytically approximate the evolution of $k_{gE}(t)$; in that model, $k_{gE}(t)$ equals k_{g1} at the first stage, it linearly increases to k_{g2} at the second stage, and then it remains equal to k_{g2} at the third stage. It is the second (nonadiabatic) stage that governs the irreversible energy transfer between the excited and absorbing effective oscillators. Indeed, due to the assumed weak coupling, the dynamics of the effective system (3a) and (3b) exhibit fast-slow time-scale separation [16], with the slow dynamics at the (critical) second stage being governed by Weber's equation, and yielding LZT and irreversible energy transfer. In turn, this analysis proves LZT wave redirection in the original nonlinear waveguides [Eq. (1)] for weak interwaveguide coupling, strong stiffness disorder, and weak viscous dissipation. From Table I, our system parameters satisfy these requirements.

Note that LZT-based wave redirection is also realized when the nonlinear intrawaveguide coupling springs are replaced by linear ones (after all, LZT is a linear quantum effect). However, the nonlinearity enables self-tunability of wave redirection to the input energy. To show this tunability, the mean (or typical) listed parameters of Table I are used to simulate the ROM [Eq. (1)] for varying initial velocities $\dot{x}_1(0+)$ of E1. The contour plot of Fig. 1(c) depicts energy penetration in the two waveguides, i.e., the maximum normalized energy of each unit cell of the waveguides for the entire simulation. There are three different regimes for the acoustics distinguished by the intensity of the impulse. In the low-energy (LE) regime (for initial velocities $\dot{x}_1(0+) < \sim 0.1$ m/s, the input energy is mainly localized in E1 and A1. In the LE regime, the nonlinear springs are not engaged due to low oscillation amplitudes; therefore, recurring energy exchanges between E1 and A1 due to 1:1 resonance dominate the acoustics in a local beat phenomenon. In the intermediate-energy (IE) regime, LZT breather redirection occurs from the excited to the absorbing waveguide through 1:1 resonance between E1 and A1 and the model of effective oscillators given in Eq. (3) holds. In the high-energy (HE) regime (for $\dot{x}_1(0+) > \sim 0.25$ m/s), intermittent localization in E1 and wave redirection occur, and much less energy is transmitted to the absorbing waveguide. In this regime, the nonlinearity significantly increases the oscillation frequency of E1, preventing sustained 1:1 resonance between E1 and A1. There is a clear boundary between the IE (LZT) and LE regimes, but not between the IE and HE regimes; this is due to viscous damping, which perturbs the wave localization in E1, yielding complex transition effects at high energies. From Fig. 1(c), LZT irreversible breather redirection from the excited to the absorbing waveguide can be realized only in the IE band, where it is robust to variations in impulse and system parameters. Lastly, we note that the nonlinear asymmetric waveguides of Fig. 1(a) support nonreciprocal acoustics, mainly in the LZT IE regime [16,22,27].

III. EXPERIMENTAL OBSERVATIONS

Guided by the ROM given in Eq. (1), we fabricate an experimental fixture of coupled nonlinear waveguides as in Fig. 2. Each unit cell is made of a U-shaped aluminum block mass grounded by a pair of thin (< 130 μm) copper-beryllium flexure springs with small intrinsic dissipative capacities [28] [cf. Fig. 2(b)]. Within the desired range of oscillation amplitudes, these flexures act as the linear grounding springs of the ROM. The softer (k_{g1}) and stiffer (k_{g2}) grounding springs of the ROM are realized by modifying the widths of the leaves of the flexures. Within the same waveguide, each unit cell is coupled to its adjacent ones by two thin 100-μm-diameter music wires (cf. Fig. 2) acting as the nonlinear coupling springs of the ROM. Indeed, a straight initially untensioned thin wire, under transverse deformation at its center, exhibits an essentially nonlinear (nonlinearizable) stiffness restoring force of approximately the third order [29] [cf. Fig. 1(b)]; however, acceptable small linear stiffness components are achieved experimentally, by minimizing the unavoidable bending effects and pretensions of the wires by means of large length-to-diameter wire ratios and our systematic assembly protocol [21,30]. Lastly, thick 1-mm-diameter spring-steel wires of length 10 cm are clamped between corresponding unit cells of both waveguides (Fig. 2) to realize the weak linear interwaveguide coupling stiffnesses k_e (cf. Fig. 1).

Accelerometers are used to measure the response of each unit cell (see the Supplemental Material [21]). The measured time series are postprocessed to obtain the energy results of Figs. 3 and 4. Regarding the actuation of the excited waveguide, the unit cell E1 is manually forced by a PCB® miniature modal impact hammer. The duration of the impulse is measured as approximately 2 ms, i.e., much smaller than the linearized natural period of the unit cell (approximately 40 ms); hence, the experimental impulse meets the computational assumption. Three different impulse intensities are considered, denoted by the

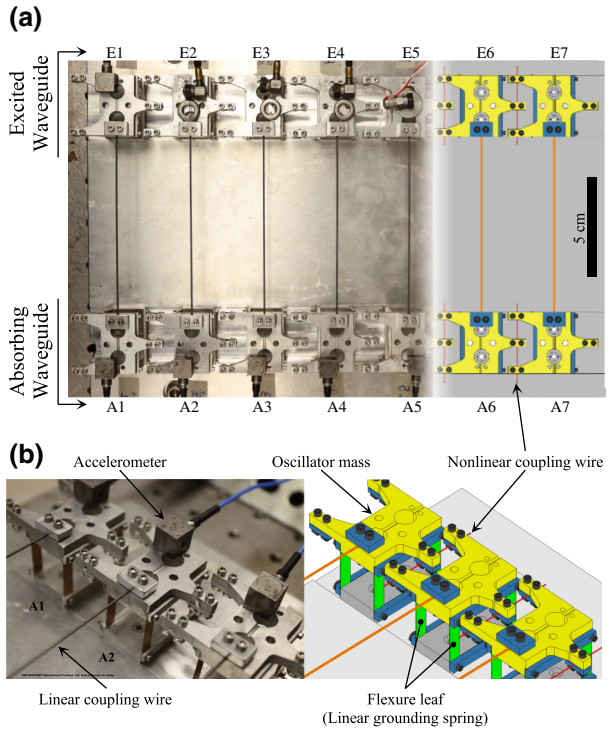

FIG. 2. The experimental fixture of the nonlinear coupled waveguides with 14 unit cells. (a) A top view, with the last four unit cells replaced by schematics for visualization. (b) Isometric (left) and schematic (right) views of unit cell A2 connected with A1 and A3; each unit cell is composed of a U-shaped aluminum block mass (yellow) grounded via a pair of flexure leaves (green), with intrawaveguide nonlinear coupling being realized by thin wires (red) and interwaveguide linear coupling by thick wires (orange).

three points L, M, and H in Fig. 1(c). The correspondence with the simulation is based on the ROM given in Eq. (1), with $F(t)$ being the experimentally measured impulse. The data from the impact hammer and the 14 accelerometers is recorded via an m + p VibPilot® dynamic analyzer. Before studying the acoustics, the stiffness and damping parameters of each unit cell are estimated by system-identification experiments (details are provided in the Supplemental Material [21]). The estimated parameter variations between the unit cells due to manufacturing and assembly are small (cf. Table I), allowing us to use mean values to simulate the experiments.

Figure 3 depicts the spatiotemporal evolution of the normalized instantaneous energy in the experimental fixture and the simulated ROM at the three excitation levels, while Fig. 4 shows the corresponding normalized instantaneous energy envelopes quantifying the energy partition in time between waveguides. The normalizations are with respect to the maximum energy attained (see the Supplemental Material [21]). At point L in Fig. 3(a), the impulsive energy becomes localized in the leading unit cells E1 and A1, being continuously and recurrently exchanged between them; this confirms the energy-penetration plot in Fig. 1(c). The localization is due to the low impulse, yielding negligibly small nonlinear intrawaveguide coupling. This is noted in Fig. 4(a) with recurrent complete energy exchanges between E1 and A1. Note the good agreement between experiment and simulation.

Breather redirection due to LZT is confirmed at point M [cf. Fig. 3(b)], both experimentally and numerically. The spatiotemporal energy evolution shows irreversible energy transmission from the excited unit cell E1 to the absorbing waveguide. It is evident in the experiments that the redirected breather reaches the end unit cell A7, while the response of the excited waveguide is negligible after the second unit cell E2. Therefore, in the LZT regime the acoustics are reduced, in effect, to a single propagating breather [27,31] in the absorbing waveguide. In fact, the breather redirection at this intermediate energy level is nearly controlled by the leading unit cells E1, A1, and A2 [16]. In this case, energy is rapidly and irreversibly transferred from E1 to A1, so the effective oscillator model given in Eq. (3) is valid and provides an accurate theoretical prediction of the irreversible energy transfer. Moreover, the results in Fig. 4(b) confirm the LZT effect.

At the HE point H [cf. Fig. 3(c)], there is a complex state of the acoustics, as within an initial stage of

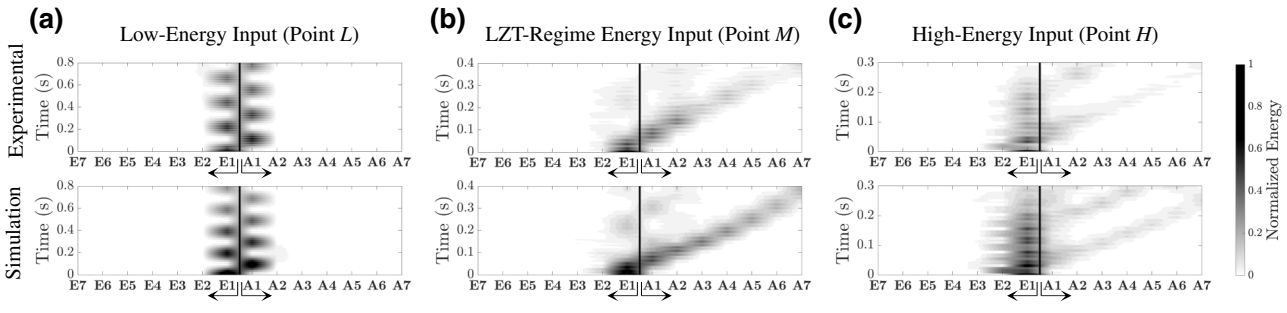

FIG. 3. The spatiotemporal evolution of the normalized energy in the experimentally tested fixture (top) and the simulated ROM (bottom) when subjected to (a) low-, (b) intermediate-, and (c) high-energy input [cf. Fig. 1(c)].

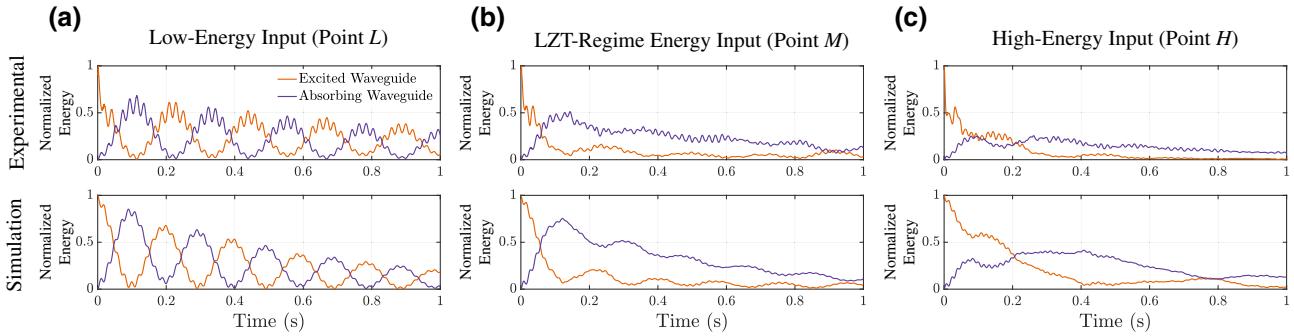

FIG. 4. The experimental (top) and simulated (bottom) envelopes of the normalized energies of the excited (orange) and absorbing (purple) waveguides as functions of time: (a)–(c) as in Fig. 3.

duration approximately 0.2 s the input energy is mainly localized in E1 and E2, with a weak propagating breather released to the absorbing waveguide. Following this stage, the energy localization in the excited waveguide almost ends and the remaining (diminished) energy is redirected to the absorbing waveguide as a weak propagating breather. In this case, viscous damping plays an important role in the acoustics: by dissipating a significant part of the localized energy in the excited waveguide (at a faster scale compared to the previous cases), it enables eventual 1:1 resonance between E1 and A1 [16,32] and, thus, breather redirection. This is confirmed both experimentally and numerically in Fig. 4(c), where up to approximately 0.2 s, the input energy is mainly localized in the leading unit cells of the excited waveguide and then released with time delay to the absorbing waveguide in a similar LZT scenario to point *M*. This, however, occurs only after the localized energy is significantly reduced due to viscous dissipation at a level at which nonlinearity becomes less dominant and 1:1 resonance between the unit cells E1 and A1 can be realized; only then can the remaining energy finally be redirected to the absorbing waveguide. Hence, at high energies there is still irreversible breather redirection from the excited to the absorbing waveguide, albeit time delayed and weaker. The model given in Eq. (3) is not applicable here, due to the initial localization in the excited waveguide.

The good agreement at all three energy levels between experiments and simulations in Fig. 3 proves the validity of the ROM given in Eq. (1) with the mean (or typical) parameter values of Table I. There is some deviation between experiments and simulations in the plots of Fig. 4, caused by postprocessing errors in estimating the initial velocity of the unit cell E1 (see the Supplemental Material [21]); these errors originate from the high drifts in the accelerometer measurements due to sudden velocity jumps immediately following the applied impulses by the impact hammer. The drift errors account for the sudden initial energy decreases in the experimental plots of Fig. 4 within milliseconds of the application of the impulse to E1 and the uniformly lower experimental energies compared to the simulated ones. Apart from this discrepancy, however, the experimental results confirm the three theoretically predicted response regimes and, more importantly, the LZT-based breather redirection in the IE regime. Lastly, the passive self-tunability of the acoustics and the irreversible breather redirection due to the strong stiffness nonlinearity are experimentally proved.

IV. CONCLUSIONS

Experimental validation of a macroscale analog of classical quantum LZT is presented and applied for irreversible wave redirection in weakly coupled and disordered nonlinear waveguides under impulse excitation. The strong stiffness nonlinearity yields passive self-tunability of the acoustics to the energy, switching between localization and wave redirection depending on the impulse intensity. Such inherent and passive self-tunable wave tailoring is not possible in linear time-invariant settings. The results highlight the efficacy of LZT-based passive wave redirection in a broad class of acoustical systems combining nonlinearity, disorder, and weak coupling, with potential applications in shock mitigation, solid state physics, ultrasonics, metamaterials, acoustic surface-wave devices, structural logic, and optics. Finally, we note that the realization of passive energy redirection inflicts a break of acoustic reciprocity in the considered lattices, which can have additional applications in nonlinear acoustics.

ACKNOWLEDGMENTS

This work was supported in part by the National Science Foundation (NSF) Emerging Frontiers Research Initiative (EFRI) through Grant No. 1741565.

C.W. and A.K. contributed equally to this work.

[1] L. D. Landau, A theory of energy transfer II, Phys. Z. Sowjetunion **2**, 19 (1932).

[2] C. Zener, Non-adiabatic crossing of energy levels, Proc. R. Soc. London. Ser. A, Containing Pap. Math. Phys. Charact. 137, 696 (1932).

[3] H. Schneider, H. Grahn, K. v. Klitzing, and K. Ploog, Resonance-Induced Delocalization of Electrons in GaAs-AlAs Superlattices, Phys. Rev. Lett. **65**, 2720 (1990).

[4] B. Rosam, K. Leo, M. Glück, F. Keck, H. Korsch, F. Zimmer, and K. Köhler, Lifetime of Wannier-Stark states in semiconductor superlattices under strong Zener tunneling to above-barrier bands, Phys. Rev. B **68**, 125301 (2003).

[5] C. Bharucha, K. Madison, P. Morrow, S. Wilkinson, B. Sundaram, and M. Raizen, Observation of atomic tunneling from an accelerating optical potential, Phys. Rev. A **55**, R857 (1997).

[6] B. P. Anderson and M. A. Kasevich, Macroscopic quantum interference from atomic tunnel arrays, Science **282**, 1686 (1998).

[7] M. Cristiani, O. Morsch, J. Müller, D. Ciampini, and E. Arimondo, Experimental properties of Bose-Einstein condensates in one-dimensional optical lattices: Bloch oscillations, Landau-Zener tunneling, and mean-field effects, Phys. Rev. A **65**, 063612 (2002).

[8] C. Sias, A. Zenesini, H. Lignier, S. Wimberger, D. Ciampini, O. Morsch, and E. Arimondo, Resonantly Enhanced Tunneling of Bose-Einstein Condensates in Periodic Potentials, Phys. Rev. Lett. **98**, 120403 (2007).

[9] H. Sanchis-Alepuz, Y. A. Kosevich, and J. Sánchez-Dehesa, Acoustic Analogue of Electronic Bloch Oscillations and Resonant Zener Tunneling in Ultrasonic Superlattices, Phys. Rev. Lett. **98**, 134301 (2007).

[10] J. Sánchez-Dehesa, H. Sanchis-Alepuz, Y. A. Kosevich, and D. Torrent, Acoustic analog of electronic Bloch oscillations and Zener tunneling, J. Acoust. Soc. Am. **120**, 3283 (2006).

[11] Z. He, S. Peng, F. Cai, M. Ke, and Z. Liu, Acoustic Bloch oscillations in a two-dimensional phononic crystal, Phys. Rev. E **76**, 056605 (2007).

[12] M. de Lima Jr, Y. A. Kosevich, P. Santos, and A. Cantarero, Surface acoustic Bloch oscillations, the Wannier-Stark ladder, and Landau-Zener tunneling in a solid, Phys. Rev. Lett. **104**, 165502 (2010).

[13] Y. A. Kosevich, L. I. Manevitch, and E. Manevitch, Vibrational analogue of nonadiabatic Landau-Zener tunneling and a possibility for the creation of a new type of energy traps, Phys.-Uspekhi **53**, 1281 (2010).

[14] L. I. Manevitch, Y. A. Kosevich, M. Mane, G. Sigalov, L. A. Bergman, and A. F. Vakakis, Towards a new type of energy trap: Classical analog of quantum Landau-Zener tunneling, Int. J. Non. Linear Mech. **46**, 247 (2011).

[15] M. Hasan, Y. Starosvetsky, A. Vakakis, and L. Manevitch, Nonlinear targeted energy transfer and macroscopic analog of the quantum Landau-Zener effect in coupled granular chains, Phys. D: Nonlinear Phenom. **252**, 46 (2013).

[16] C. Wang, S. Tawfick, and A. F. Vakakis, Irreversible energy transfer, localization and non-reciprocity in weakly coupled, nonlinear lattices with asymmetry, Phys. D: Nonlinear Phenom. **402**, 132229 (2020).

[17] Y. A. Kosevich, L. Manevitch, and A. Savin, Y. A. Kosevich, L. Manevitch, and A. Savin, Energy transfer in coupled nonlinear phononic waveguides: Transition from wandering breather to nonlinear selftrapping, in *Journal of Physics: Conference Series* Vol. 92 (Institute of Physics and IOP Publishing Limited, Paris, France, 2007), p. 012093.

[18] Y. A. Kosevich, L. I. Manevitch, and A. V. Savin, Wandering breathers and self-trapping in weakly coupled nonlinear chains: Classical counterpart of macroscopic tunneling quantum dynamics, Phys. Rev. E **77**, 046603 (2008).

[19] Y. A. Kosevich, L. I. Manevitch, and A. V. Savin, Energy transfer in weakly coupled nonlinear oscillator chains: Transition from a wandering breather to nonlinear self-trapping, J. Sound Vib. **322**, 524 (2009).

[20] Y. Starosvetsky, M. A. Hasan, A. F. Vakakis, and L. I. Manevitch, Strongly nonlinear beat phenomena and energy exchanges in weakly coupled granular chains on elastic foundations, SIAM J. Appl. Math. **72**, 337 (2012).

[21] See the Supplemental Material at http://link.aps.org/supplemental/10.1103/PhysRevApplied.14.034053 for tables of identified parameters of the fixture and detailed explanations related to the assembly protocols, the system-identification experiments, the postprocessing of measurements, and videos of wave localization and LZT wave redirection.

[22] A. Mojahed, J. Bunyan, S. Tawfick, and A. F. Vakakis, Tunable Acoustic Nonreciprocity in Strongly Nonlinear Waveguides with Asymmetry, Phys. Rev. Appl. **12**, 034033 (2019).

[23] H. E. Rauch, F. Tung, and C. T. Striebel, Maximum likelihood estimates of linear dynamic systems, AIAA J. **3**, 1445 (1965).

[24] K. Murphy, Kalman filter toolbox for MATLAB, Computer Science and Artificial Intelligence Laboratory, MIT (1998).

[25] S. B. Kim, B. Spencer Jr, and C.-B. Yun, Frequency domain identification of multi-input, multi-output systems considering physical relationships between measured variables, J. Eng. Mech. **131**, 461 (2005).

[26] D. J. Ewins, *Modal Testing: Theory, Practise and Application* (Wiley, New York, 2009),2nd ed.

[27] A. Mojahed, O. V. Gendelman, and A. F. Vakakis, Breather arrest, localization, and acoustic non-reciprocity in dissipative nonlinear lattices, J. Acoust. Soc. Am. **146**, 826 (2019).

[28] M. Ashby and A. Greer, Metallic glasses as structural materials, Scr. Mater. **54**, 321 (2006).

[29] D. M. McFarland, L. A. Bergman, and A. F. Vakakis, Experimental study of non-linear energy pumping occurring at a single fast frequency, Int. J. Non. Linear Mech. **40**, 891 (2005).

[30] A. F. Vakakis, O. V. Gendelman, L. A. Bergman, D. M. McFarland, G. Kerschen, and Y. S. Lee, *Nonlinear Targeted Energy Transfer in Mechanical and Structural Systems* (Springer Science & Business Media, Dordrecht, 2008), Vol. 156.

[31] A. Mojahed and A. F. Vakakis, Certain aspects of the acoustics of a strongly nonlinear discrete lattice, Nonlinear Dyn. **99**, 643 (2020).

[32] L. Manevitch, New approach to beating phenomenon in coupled nonlinear oscillatory chains, Arch. Appl. Mech. **77**, 301 (2007).